

Device Simulation of Carrier Transport through Grain Boundaries in Lightly Doped Polysilicon Films and Dependence on Dopant Density

Mutsumi KIMURA*, Satoshi INOUE, Tatsuya SHIMODA and Toshiyuki SAMESHIMA¹

Base Technology Research Center, Seiko Epson Corporation, 281 Fujimi, Nagano 399-0293, Japan

¹Department of Electrical and Electric Engineering, Tokyo University of Agriculture and Technology, 2-24-16 Nakamachi, Koganei 184-8588, Japan

(Received November 14, 2000; accepted for publication June 11, 2001)

Carrier transport through grain boundaries in lightly doped polysilicon films has been analyzed using device simulation. Grain boundary defects not only trap and reduce free carriers, but also form potential barriers and interfere with carrier movement. The dependence of the energy band, carrier density, potential barrier and electric conductivity on the dopant density has been closely investigated. The carrier density increases monotonically as the dopant density increases. The potential barrier height reaches its maximum value when the dopant density is roughly equal to the defect density. The electric conductivity dramatically increases around the specific dopant density that is sensitive to the defect density. The actual defect density can be extracted by comparing the experimental electric conductivity with the simulated one. The device simulation is more reliable than analytical methods, since it can accurately handle phenomena such as the energy distribution and partial occupation of the grain boundary defects, partial ionization of the dopants, gradual depletion and so forth, which are neglected or approximated in the analytical methods.

KEYWORDS: device simulation, carrier transport, grain boundary, lightly doped, polysilicon, potential barrier, electric conductivity, dopant, defect

1. Introduction

In polysilicon (poly-Si) thin-film transistors (TFTs), carrier transport occurs in poly-Si films that include grains and grain boundaries. In particular, laser-crystallized poly-Si films have few defects in the grains and many defects at the grain boundaries in comparison with other poly-Si films. In order to understand the working of the poly-Si TFTs, it is necessary to clarify the mechanism of the carrier transport through the grain boundaries in the poly-Si films. One of the most effective methods for clarifying this mechanism is to evaluate lightly doped poly-Si films.^{1–5} In the evaluation of lightly doped poly-Si films, no voltage is applied along the poly-Si film depth, and no carriers are concentrated at the oxide-silicon interface. Therefore, the effect of the oxide-silicon interface on the carrier transport is negligible, while that of the grain boundaries is dominant. Moreover, since the changes of electrical potential and carrier density along the poly-Si film depth are negligible, two-dimensional subjects can be treated as one-dimensional subjects. From the viewpoint of sample fabrication, since only poly-Si films with some contact pads are required, it is easier to fabricate them than to fabricate poly-Si TFTs.

There are some reports that have analyzed the carrier transport in lightly doped poly-Si films.^{6–9} Since they are based on analytical methods, some assumptions and approximations are required, which cause errors. Recently, a paper was reported by the authors, which was based on device simulation in order to precisely analyze the carrier transport in poly-Si films.¹⁰ The mechanism of the carrier transport in the poly-Si films was clarified, and the dependence on the defect density was analyzed.

The objectives of this study are to analyze the carrier transport through the grain boundaries in the lightly doped poly-Si films using the device simulation and closely investigate the dependence of the energy band, carrier density, potential bar-

rier and electric conductivity on the dopant density. Experiments are carried out in order to extract the actual defect density by comparing the experimental electric conductivity with the simulated one. The carrier density, potential barrier and electric conductivity obtained using the device simulation are compared with those acquired using an analytical method. It is expected that the device simulation is more reliable than the analytical methods, since the device simulation can accurately handle phenomena such as the energy distribution and partial occupation of the grain boundary defects, partial ionization of the dopants, gradual depletion and so forth, which are neglected or approximated in the analytical methods.

2. Simulation

Figure 1 shows the carrier transport in the lightly doped poly-Si film with the grain boundary defects. Dopants are distributed uniformly over the entire poly-Si film, while the

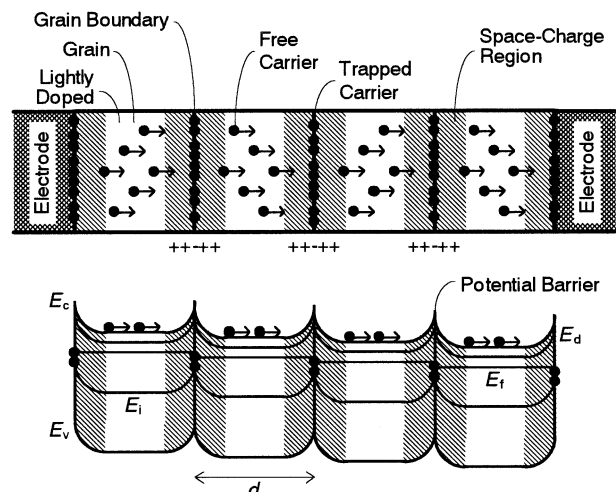


Fig. 1. Carrier transport in the lightly doped poly-Si film with the grain boundary defects.

*E-mail address: kimura.mutsumi@exc.epson.co.jp

defects are localized at the grain boundaries. When the donor-type dopants are ionized, free electron carriers are generated in the conduction band. The free carriers are trapped at the grain boundary defects and decrease. The grain boundary defects are charged negatively, and positive charges balanced with negative charges at the grain boundary defects are induced on both sides of the grain boundaries in order to preserve charge neutrality. That is, the free carriers decrease on both sides of the grain boundaries, and space-charge regions are formed by the positive charges of the dopant ions. These space-charge regions form potential barriers at the grain boundaries. The potential barriers bend the energy band upward at the grain boundaries, shift the relationship between the defect energy and Fermi level, affect the occupation probability of the grain boundary defects, change the negative charges at the grain boundary defects and circularly make the potential barrier higher or lower. Therefore, the potential barriers and occupation probability are determined self-consistently. It is concluded that the grain boundary defects influence the carrier transport by two mechanisms. The first mechanism is to trap and reduce free carriers. The second mechanism is to form potential barriers and interfere with the free carrier movement. Only thermally activated free carriers can travel through the potential barriers.

As shown in Fig. 1, the grain size is defined by d , and four grains and three grain boundaries are assumed. This structure can be assumed to be a part of a longer poly-Si film. The dopant density varies on the order of 10^{17} – 10^{20} cm^{-3} , and the dopant energy, E_d , is 0.04 eV below the bottom of the conduction band, E_c . The energy distribution of the grain boundary defects is described by the Gaussian function as follows.

$$N_t(E) = N_1 \exp\{-(E - E_1)/E_2\}^2 \quad (1)$$

Here, E , N_1 , E_1 and E_2 are the energy in the energy gap and Gaussian parameters, respectively. The total defect density is acquired by integrating eq. (1) along the energy. The defect density varies in the plane density on the order of 10^{12} – 10^{15} cm^{-2} , which corresponds to the volume density on the order of 10^{17} – 10^{20} cm^{-3} , if it is assumed that the grain boundary defects are distributed uniformly over the entire poly-Si film. Although the defect density is indicated using the volume density in order to compare it with the dopant density in the following sections, the grain boundary defects are localized at the grain boundaries. For as-crystallized poly-Si films, the defect density is very high as described above, E_1 is 0 eV, which means that the grain boundary defects are distributed around the midgap in the energy gap, and E_2 is 0.15 eV, which means that the Gaussian width is 0.3 eV. This high defect density around the midgap is confirmed by a high potential barrier measured in a previous experiment.⁵⁾ This is because the defect density has to be high in order to form the high potential barrier and because it has to be distributed around the midgap in order to trap the free carriers even after the high potential barrier bends the energy band upward at the grain boundaries. Acceptor-like states are defined as defect states that are neutral or negatively charged according to the Fermi level. Donor-like states are also defined as defect states that are neutral or positively charged. It is assumed that the defect density of the acceptor-like states and that of the donor-like states are the same. This assumption leads to the characteristics that the Fermi level is located at the midgap

for intrinsic poly-Si films and that a flat-band condition is acquired when no voltage is applied. Since these characteristics are often observed in poly-Si TFTs, this assumption seems to be valid. A voltage of 0.1 V is applied to electrodes on both sides of the poly-Si film in order to induce an electric current and to calculate electric conductivity.

Device simulations can accurately handle phenomena related to the mechanisms described above without any approximations.^{11–13)} In the device simulation, the following equations are utilized.

$$\Delta\psi = -\rho/\varepsilon \quad (2)$$

$$\nabla \cdot (-n_n \mu_n \mathbf{E} - D_n \nabla n_n) - G = 0 \quad (3)$$

$$\nabla \cdot (-n_p \mu_p \mathbf{E} - D_p \nabla n_p) - G = 0 \quad (4)$$

Equation (2) is the Poisson equation for calculating electrical potential. Equations (3) and (4) are the continuous equations for calculating carrier transport based on the drift-diffusion model for electrons and holes, respectively. The following equations are also utilized.

$$n_d = N_d / \{1 + \exp[(E_f - E_d)/(kT)]\} \quad (5)$$

$$n_{ta} = \int N_{ta}(E) / \{1 + \exp[(E - E_f)/(kT)]\} dE \quad (6)$$

$$n_{td} = \int N_{td}(E) / \{1 + \exp[(E_f - E)/(kT)]\} dE \quad (7)$$

Equations (5), (6) and (7) are the equations for calculating the occupied state density by considering the occupation probability based on the Fermi-Dirac statistics for the donors, acceptor-like states and donor-like states, respectively. n_d and N_d are the occupied state density and total density for the donors, respectively. n_{ta} , $N_{ta}(E)$, n_{td} and $N_{td}(E)$ are the occupied state density and energy distribution of the grain boundary defects for the acceptor-like states and donor-like states, respectively. The following equation for calculating the total charge density is circularly substituted into eq. (2).

$$\rho = q(-n_n + n_p + n_d - n_{ta} + n_{td}) \quad (8)$$

In the device simulation, a structure is divided into many meshes, and eqs. (2)–(8) are formulated at each mesh. By iterating to solve these equations till the convergence is achieved, the carrier density and electrical potential can be calculated. Finally, the energy band, carrier density, potential barrier, electric conductivity and so forth can be calculated. The authors utilize a device simulator, Atlas, which applies finite-differential methods to solve eqs. (2)–(4).¹³⁾ It is vended by Silvaco International and is based on the algorithm of Pisces, which was developed at Stanford University and has been widely utilized as a standard simulator for semiconductor devices. The procedure of the device simulation has been reported previously in more detail.¹⁰⁾

3. Experimental

Experiments were carried out^{2,4,14)} in order to extract the actual defect density by comparing the experimental electric conductivity with the simulated one. First, an amorphous-silicon film was formed using low-pressure chemical vapor deposition to a 50 nm thickness. Phosphorus atoms were implanted with variations of the doping density. The amorphous-silicon film was crystallized using a XeCl excimer

laser for laser energies such as 220, 340 and 460 mJ/cm² to form a poly-Si film, and the phosphorus atoms were activated simultaneously. It is known that the defect density changes as the laser energy changes.¹⁻⁵ The poly-Si film was patterned and aluminum electrodes were fabricated. Next, a voltage was applied to the aluminum electrodes in order to induce an electric current and to calculate the electric conductivity. Finally, the grain sizes of the poly-Si films were measured using a method such as scanning electron microscopy or tunneling electron microscopy.

4. Results

The dependence of the energy band, carrier density, potential barrier and electric conductivity on the dopant density have been closely investigated using the device simulation.

4.1 Energy band

Figure 2 shows the dependence of the energy band with variations of the dopant density. The grain size is 50 nm, and the defect density is $2 \times 10^{18} \text{ cm}^{-3}$. The bottom of the conduction band, E_c , for each dopant density is shown by overlapping the Fermi level, E_f . Although the shapes of the Fermi level for each dopant density are not precisely identical, only the Fermi level for one dopant density is shown in order to avoid complicating the figure. Figure 3 shows the dependence of the carrier density with variations of the dopant density. In the middle of the grains, for a low dopant density below $2 \times 10^{18} \text{ cm}^{-3}$, E_c is distant from E_f , and the carrier density is low because the dopant density is lower than the defect density and most free carriers are trapped in the grain boundary defects. As the dopant density increases above $2 \times 10^{18} \text{ cm}^{-3}$, E_c comes close to E_f , and the carrier density increases to the same order as the dopant density because the dopant density becomes higher than the defect density and more free carriers are generated. On the other hand, at the grain boundaries, for all dopant densities, the potential barriers are formed, E_c is further distant from E_f than in the middle of grains, and the carrier density is lower. These phenomena can be explained from a different viewpoint as follows. The potential barriers are formed at the grain boundaries, E_c is distant from E_f , and the carrier density is low. The shapes of the potential barrier

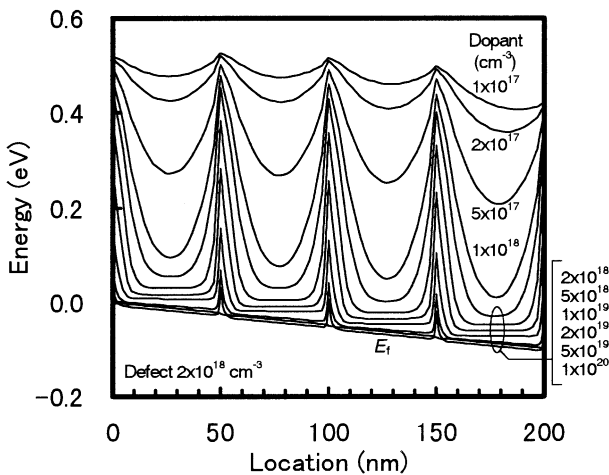


Fig. 2. Dependence of the energy band with variations of the dopant density.

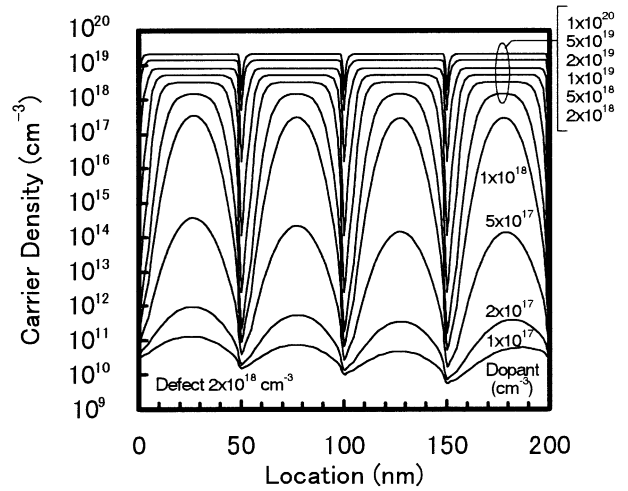


Fig. 3. Dependence of the carrier density with variations of the dopant density.

and carrier density are quite different for each dopant density. In particular, neighboring potential barriers are connected for a low dopant density below $2 \times 10^{18} \text{ cm}^{-3}$ because the space-charge regions spread to the entire grains in order to induce the positive charges balanced with the negative charges at the grain boundary defects and the neighboring space-charge regions are also connected.

4.2 Carrier density

Figure 4 shows the dependence of the carrier density in the middle of the grains on the dopant density with variations of the defect density. For a low dopant density below $2 \times 10^{17} \text{ cm}^{-3}$, the carrier density is low because most free carriers are trapped in the grain boundary defects. As the dopant density increases above $1 \times 10^{18} \text{ cm}^{-3}$, the carrier density increases because more free carriers are generated. As a result, it is found that the dependence is a monotonic increase. It is interesting that the dependence does not change significantly as the defect density changes. This is because the carrier density in the middle of the grains is not significantly influenced

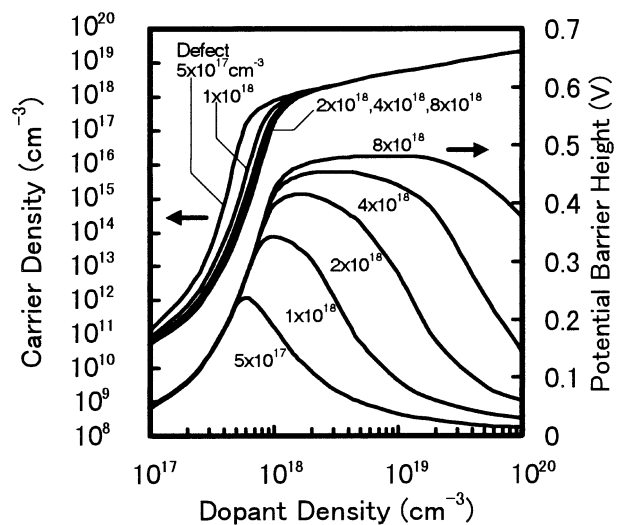


Fig. 4. Dependence of the carrier density in the middle of the grains and potential barrier height on the dopant density with variations of the defect density.

by the defect density for a grain size of 50 nm. This seems different from the case for smaller grain sizes.¹⁰⁾ It is also interesting that the carrier density is slightly lower than the dopant density even for a high dopant density above $1 \times 10^{18} \text{ cm}^{-3}$. This is because only some of the dopants are ionized according to the ionization rate when the dopant energy is similar to the Fermi level.

4.3 Potential barrier

Figure 4 also shows the dependence of the potential barrier height on the dopant density with variations of the defect density. For a low defect density such as $5 \times 10^{17} \text{ cm}^{-3}$ and a low dopant density below $2 \times 10^{17} \text{ cm}^{-3}$, the potential barrier is low because the space-charge regions spread to the entire grains but the space-charge density is very low. Only a part of the grain boundary defects is charged negatively because the total space charge, which is the product of the space-charge density and space-charge region width, has to be balanced with the negative charges at the grain boundary defects in order to preserve the charge neutrality. As the dopant density increases, the potential barrier increases because the space-charge density increases. For a dopant density of $5 \times 10^{17} \text{ cm}^{-3}$ that is the same as the defect density, the space-charge regions still spread to the entire grains, and almost all of the grain boundary defects are charged negatively. For a high dopant density such as $1 \times 10^{18} \text{ cm}^{-3}$, the space-charge density still increases but the space-charge region width narrows in order to maintain the total space charge because the grain boundary defects cannot be charged more negatively. The potential barrier decreases again because the electrical potential is approximately proportional to the space-charge density and the square of the space-charge region width, which is found by integrating eq. (2) with a location, and the effect of the space-charge region width is dominant over that of the space-charge density. As a result, the potential barrier height reaches its maximum value when the dopant density is roughly equal to the defect density. On the other hand, for a high defect density such as $8 \times 10^{18} \text{ cm}^{-3}$ and a low dopant density below $2 \times 10^{17} \text{ cm}^{-3}$, the potential barrier is low for the same reason as for a low defect density. As the dopant density increases to 1×10^{18} – $2 \times 10^{19} \text{ cm}^{-3}$, the potential barrier increases and becomes saturated because the defect energy becomes similar to the Fermi level and the grain boundary defects cannot be charged more negatively. For a high dopant density of $1 \times 10^{20} \text{ cm}^{-3}$, the potential barrier decreases also for the same reason as for a low defect density.

4.4 Electric conductivity

Figure 5 shows the dependence of the electric conductivity on the dopant density with variations of the defect density. The electric conductivity is determined by the carrier density and potential barrier described above. For a low dopant density, the electric conductivity is low because the carrier density is low. As the dopant density increases, the electric conductivity remains low because the carrier density increases but the potential barrier also increases. As the dopant density increases further, the electric conductivity dramatically increases because the carrier density remains high but the potential barrier starts decreasing. As a result, it is found that the electric conductivity dramatically increases around the

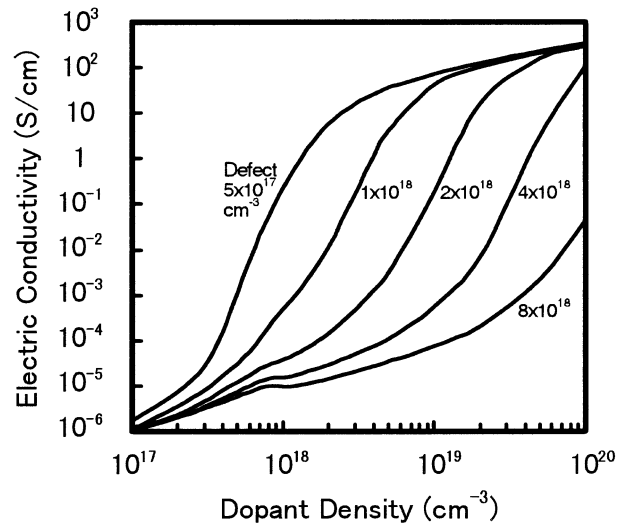


Fig. 5. Dependence of the electric conductivity on the dopant density with variations of the defect density.

specific dopant density. This specific dopant density corresponds to the dopant density where the potential barrier starts decreasing and strongly depends on the defect density. It is interesting that the dependence is quite sensitive to the defect density. The other interesting point is the negative dependence of the electric conductivity on the dopant density. For high defect densities such as 4×10^{18} and $8 \times 10^{18} \text{ cm}^{-3}$ and a dopant density around $8 \times 10^{17} \text{ cm}^{-3}$, the electric conductivity decreases although the dopant density increases. This is because the rapid increase of the potential barrier surpasses the increase of the carrier density.

5. Discussion

5.1 Extraction of defect density

The actual defect density can be extracted by comparing the experimental electric conductivity with the simulated one. Figure 6 shows the experimental electric conductivity with variations of the laser energy for crystallization and simulated

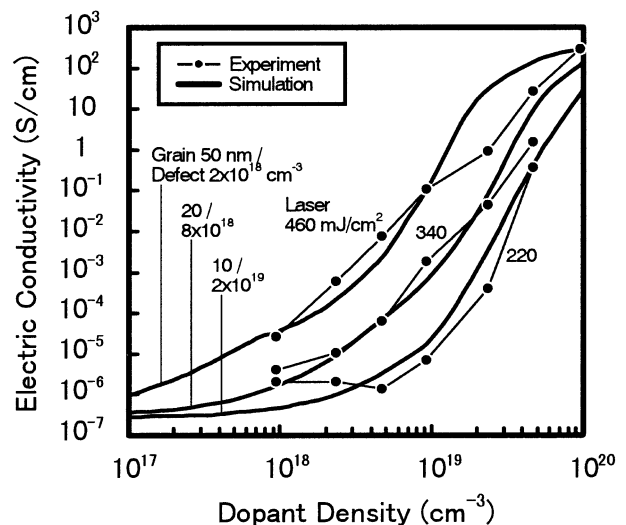


Fig. 6. Experimental electric conductivity with variations of the laser energy for crystallization and simulated electric conductivity with the extracted defect density.

electric conductivity with the extracted defect density. The grain sizes were 10, 20 and 50 nm for laser energies of 220, 340 and 460 mJ/cm², respectively. Using these grain sizes, the dependence of the electric conductivity on the dopant density with variations of the defect density was simulated as shown in Fig. 5. Since the dependence of the electric conductivity on the dopant density is quite sensitive to the defect density, it is possible to extract the actual defect density by comparing the experimental electric conductivity with the simulated one. The extracted defect densities for laser energies of 220, 340 and 460 mJ/cm² are the volume densities of 2×10^{19} , 8×10^{18} and 2×10^{18} cm⁻³, which correspond to the plane densities of 2×10^{13} , 1.6×10^{13} and 1×10^{13} cm⁻², respectively. It is very interesting that the actual defect density can be extracted using a very simple structure such as a lightly doped poly-Si film and a very easy measurement such as that of electric conductivity.

As shown in Fig. 6, it is found that the simulated dependence of the electric conductivity agrees with the experimental one. This is a part of the evidence suggesting that this simulation has correctly handled the mechanism of the carrier transport in the poly-Si films. However, there are still differences between the simulated dependence of the electric conductivity and experimental one, particularly for a laser energy such as 220 mJ/cm² and a low dopant density such as 1×10^{18} cm⁻³ and for a laser energy such as 460 mJ/cm² and a high dopant density such as 1×10^{19} cm⁻³. The authors believe that one reason for the difference under the former condition is the error in the experiment. It is difficult to measure small electric current under this condition because the variation between different devices, which may be caused by contamination of impurities, is large and fluctuation during the measurement, which may be caused by the dynamic noise of trap-detrap of defects¹⁵⁾ and by local Joule heating, is also large. The authors believe that other reasons for these differences are the assumptions in the device simulation. First, the carrier transport occurs in three-dimensional structures in the actual poly-Si films.¹⁶⁾ The carrier transport is winding because the grain boundaries compose networks. However, it is assumed that the carrier transport occurs in one-dimensional structures in the device simulation. Second, the grain size is different for every grain in the actual poly-Si films. However, it is assumed that the grain size is the same for every grain in the device simulation. In particular, as the laser energy becomes higher, not only the grain size but also its variation tends to become larger. If there is a small grain region in the three-dimensional path of the carrier transport, this region is dominant for the electric conductivity and lowers it. The authors believe that this is main reason for the difference under the latter condition.

5.2 Comparison between device simulation and analytical method

Figure 7 shows the comparison of the carrier densities and potential barrier heights obtained using the device simulation and analytical method.⁶⁻⁹⁾ The device simulation is more reliable than the analytical methods, since the device simulation can accurately handle phenomena, which are neglected or approximated in the analytical methods. The first phenomenon is the energy distribution and partial occupation of the grain boundary defects. As shown by eq. (1), the grain boundary

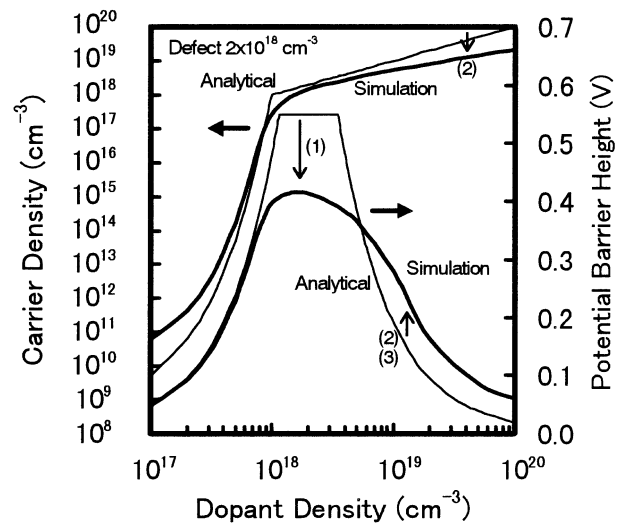


Fig. 7. Comparison of the carrier densities and potential barrier heights obtained using the device simulation and analytical method. The difference is caused by the (1) energy distribution and partial occupation of the grain boundary defects, (2) partial ionization of the dopants and (3) gradual depletion.

defects are not distributed at one fixed energy level, but are distributed continuously in the energy. Moreover, only some of the grain boundary defects trap the free carriers and are charged according to the occupation probability. The difference between the device simulation and analytical methods caused by this phenomenon is conspicuous when the defect energy is similar to the Fermi level. This condition occurs when the potential barrier height is near its maximum value because the midgap comes close to the Fermi level due to band bending at the grain boundary and the grain boundary defects are distributed around the midgap. This difference is indicated by (1) in Fig. 7. In the analytical method, since all grain boundary defects are assumed to be charged, the potential barrier is relatively high. On the other hand, in the device simulation, since only some of the grain boundary defects are charged according to the occupation probability, the potential barrier is relatively low. The second phenomenon is the partial ionization of the dopants. Only some of the dopants are ionized according to the ionization rate. The difference is conspicuous when the dopant energy is similar to the Fermi level. This condition occurs when the dopant density is high because the Fermi level comes close to the bottom of the conduction band and the dopant energy is 0.04 eV below the bottom of the conduction band. This difference is indicated by (2) in Fig. 7. In the analytical method, since all of the dopants are assumed to be ionized, the carrier density is relatively high. The space-charge density is relatively high, the space-charge region is relatively narrow, and the potential barrier is relatively low. On the other hand, in the device simulation, since only some of the dopants are ionized according to the ionization rate, the potential barrier is relatively high. The third phenomenon is the gradual depletion. As shown in Fig. 3, the poly-Si films are not depleted abruptly near the grain boundaries, but are depleted gradually, that is, the carrier density decreases gradually. The difference is conspicuous when the bottom of the conduction band is similar to the Fermi level. This condition also occurs when the dopant density is high. This difference is indicated by (3) in Fig. 7. In

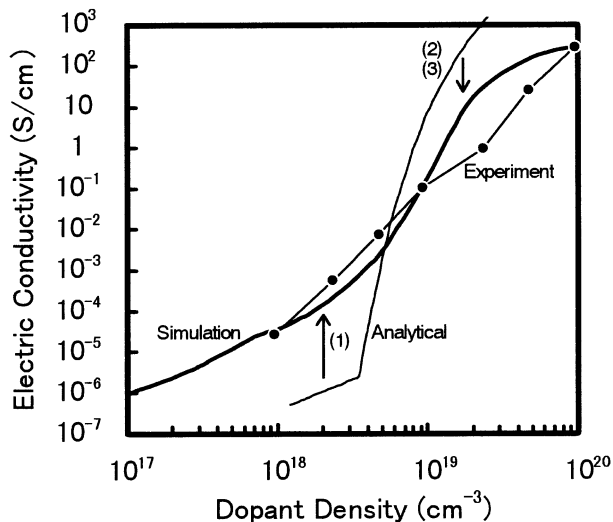


Fig. 8. Comparison of the electric conductivities obtained using the device simulation and analytical method with the experimental electric conductivity. The difference is caused by the (1) energy distribution and partial occupation of the grain boundary defects, (2) partial ionization of the dopants and (3) gradual depletion.

the analytical methods, since the abrupt depletion approximation is utilized, the space-charge density is relatively high, the space-charge region width is relatively narrow, and the potential barrier is relatively low. On the other hand, in the device simulations, since the gradual depletion is utilized, the potential barrier is relatively high.

Figures 8 shows the comparison of the electric conductivities obtained using the device simulation and analytical method⁶⁻⁹⁾ with the experimental electric conductivity. The difference is caused by the three phenomena described above. As indicated by (1) in Fig. 8, the simulated electric conductivity is much higher than the analytical one for a dopant density below $5 \times 10^{18} \text{ cm}^{-3}$. This is because the simulated potential barrier is lower than the analytical one, as indicated by (1) in Fig. 7. As indicated by (2) and (3) in Fig. 8, the simulated electric conductivity is much lower than the analytical one for a dopant density above $5 \times 10^{18} \text{ cm}^{-3}$. This is because the simulated carrier density is lower than the analytical one and the simulated potential barrier is higher than the analytical one, as indicated by (2) and (3) in Fig. 7. By comparing the simulated and analytical dependence of the electric conductivity with the experimental one, it is found that not the analytical but the simulated dependence of the electric conductivity agrees with the experimental one.

6. Conclusions

Carrier transport through grain boundaries in lightly doped poly-Si films has been analyzed using device simulation. The dependence of the energy band, carrier density, potential barrier and electric conductivity on the dopant density has been closely investigated. The actual defect density can be extracted by comparing the experimental electric conductivity with the simulated one. The device simulation is more reliable than analytical methods, since the device simulation can accurately handle phenomena, which are neglected or approximated in the analytical methods.

The evaluation of lightly doped poly-Si films is applicable

to process diagnostics. As described above, the mechanism of the carrier transport through the grain boundaries in the poly-Si films is simpler than that in poly-Si TFTs, it is easier to fabricate lightly doped poly-Si films than to fabricate poly-Si TFTs, and the actual defect density can be extracted. Therefore, the evaluation of lightly doped poly-Si films can be a very simple, quick and therefore useful method for the process diagnostics.

In the lightly doped poly-Si films, the free carriers are generated by the dopants. On the other hand, in the poly-Si TFTs, the free carriers are generated by the application of gate voltage. However, the phenomena are analogous when the carrier density in the poly-Si films is the same as that in the poly-Si TFTs. In the subthreshold region of the poly-Si TFTs, the free carrier density at the oxide-silicon interface is estimated to be on the order of $10^{10} - 10^{16} \text{ cm}^{-3}$,¹⁷⁾ which corresponds to a dopant density below 10^{18} cm^{-3} , as shown in Fig. 4. The potential barrier increases as the dopant density increases for this dopant density. Therefore, the large subthreshold swing parameter of the poly-Si TFTs may be caused not only by trapping and reducing free carriers, but also by forming potential barriers and interfering with carrier movement. On the other hand, in the on region, the free carrier density is estimated to be on the order of $10^{16} - 10^{19} \text{ cm}^{-3}$,¹⁷⁾ which corresponds to a dopant density above 10^{18} cm^{-3} . As shown in Fig. 5, the electric conductivity dramatically changes as the defect density changes for this dopant density. Therefore, the on-current of the poly-Si TFTs strongly depends on the defect density. It is important to reduce the defect density in order to improve the on-current.

With respect to future research, the authors would like to measure the dependence of the electric conductivity on temperature and calculate the activation energy with variations of the dopant density for the lightly doped poly-Si films or variations of the gate voltage for the poly-Si TFTs. Since the potential barrier height is reflected by the activation energy, the results of this paper will be confirmed by this measurement.

Acknowledgements

The authors wish to thank Mr. Seiichiro Higashi of Seiko Epson Corporation for providing the lightly doped poly-Si films and experimental data, Dr. Ramesh Kakkad, formerly of Seiko Epson Corporation for useful discussion on the mechanism of the carrier transport through the grain boundaries in the poly-Si films and Professor Piero Migliorato of the University of Cambridge for useful discussions on the workings of the poly-Si TFTs and defects. The authors also wish to thank the members of the Base Technology Research Center of Seiko Epson Corporation, the Epson Cambridge Laboratory, Professor Migliorato's group at the University of Cambridge and the LT Business Development Center of Seiko Epson Corporation.

- 1) T. Sameshima, K. Saito, M. Sato, A. Tajima and N. Takashima: Jpn. J. Appl. Phys. **36** (1997) L1360.
- 2) S. Higashi, K. Ozaki, K. Sakamoto, Y. Kano and T. Sameshima: Jpn. J. Appl. Phys. **38** (1999) L857.
- 3) T. Sameshima, K. Saitoh, N. Aoyama, S. Higashi, M. Kondo and A. Matsuda: Jpn. J. Appl. Phys. **38** (1999) 1892.
- 4) S. Higashi: Dig. Tech. Pap. Int. Workshop on Active-Matrix Liquid-Crystal Displays 1999, Tokyo, p. 225.

- 5) K. Sakamoto, Y. Tsunoda, T. Watanabe, K. Asada, T. Mohri, T. Sameshima and S. Higashi: Ext. Abstr. (60th Autumn Meet. 1999); The Japan Society of Applied Physics, Tokyo, p. 804 [in Japanese].
- 6) J. Y. W. Seto: J. Appl. Phys. **46** (1975) 5247.
- 7) G. Bacarani, B. Ricco and G. Spadini: J. Appl. Phys. **49** (1978) 5565.
- 8) P. V. Evans and S. F. Nelson: J. Appl. Phys. **69** (1991) 3605.
- 9) T. Kamins: *Polycrystalline Silicon for Integrated Circuits and Displays* (Kluwer Academic Publishers, Boston, 1998) 2nd ed., Chap. 5, p. 199.
- 10) M. Kimura, S. Inoue, T. Shimoda and T. Sameshima: Jpn. J. Appl. Phys. **40** (2001) 49.
- 11) S. Selberherr: *Analysis and Simulation of Semiconductor Devices* (Springer-Verlag, Vienna, 1984).
- 12) K. Taniguchi: *Latest Semiconductor Process and Device Simulation Technology* (Realize Inc., Tokyo, 1990) [in Japanese].
- 13) *Atlas User's Manual, Device Simulation Software* (Silvaco International, Santa Clara, 2000).
- 14) S. Higashi: private communication (2000).
- 15) C. T. Angelis, C. A. Dimitriadis, J. Brini, G. Kamarinos, V. K. Gueorguiev and T. E. Ivanov: IEEE Trans. Electron Devices **46** (1999) 968.
- 16) M. Kimura, S. Inoue, T. Shimoda and T. Sameshima: Jpn. J. Appl. Phys. **40** (2001) L97.
- 17) M. Kimura, R. Nozawa, S. Inoue, T. Shimoda, B. O.-K. Lui, S. W.-B. Tam and P. Migliorato: Jpn. J. Appl. Phys. **40** (2001) 112.